Brownian Dynamics Simulations of Supercoiled DNA with Bent Sequences

Giuseppe Chirico* and Jörg Langowski#
*Istituto Nazionale Fisica della Materia, Dipartimento di Fisica, Università degli Studi di Milano, I-20133 Milan, Italy, and #Abteilung Biophysik der Makromoleküle (0830), Deutsches Krebsforschungszentrum, Im Neuenheimer Feld 280, D-69120 Heidelberg, Germany

ABSTRACT The recently presented Brownian dynamics model for superhelical DNA is extended to include local curvature of the DNA helix axis. Here we analyze the effect of a permanent bend on the structure and dynamics of an 1870-bp superhelix with $\Delta Lk = -10$. Furthermore, we define quantitative expressions for computing structural parameters such as loop positions, superhelix diameter, and plectonemic content for trajectories of superhelical DNA, and assess the convergence toward global equilibrium. The structural fluctuations in an interwound superhelix, as reflected in the change in end loop positions, seem to occur by destruction/creation of loops rather than by a sliding motion of the DNA around its contour. Their time scale is on the order of 30–100 μs. A permanent bend changes the structure and the internal motions of the DNA drastically. The position of the end loop is fixed at the permanent bend, and the local motions of the chain are enhanced near the loops. A displacement of the bend from the end loop to a position inside the plectonemic part of the superhelix results in the formation of a new loop and the disappearance of the old one; we estimate the time involved in this process to be about 0.5 ms.

INTRODUCTION

The long-range ordering of DNA is determined to a great extent by the interplay between torsional stress in the DNA and local structural changes such as DNA curvature, induced by bound proteins or intrinsic particular sequences. Torsional stress causes the folding of DNA into a plectonemic superhelix; in such a structure, intramolecular interactions are different from those in unstressed DNA, as witnessed by supercoiling-induced DNA looping (Borowiec et al., 1987) and by recent model calculations (Klenin et al., 1995; Vologodskii et al., 1992). It is known that DNA supercoiling influences the activity of pro- and eukaryotic promoters, and it has been hypothesized that DNA curvature could control the global structure of the superhelix and therefore modulate interactions between distant sites (Klenin et al., 1995; Kremer et al., 1993; Laundon and Griffith, 1988; ten Heggeler-Bordier et al., 1992; Zhang et al., 1994). The effect of bends on DNA supercoiling has been reviewed recently (Yang et al., 1995), and it has been emphasized that for DNAs longer than the persistence length, fluctuations must be taken into account for a realistic description of the structure dynamics (Langowski et al., 1996). After the assessment of the effect of curved inserts on the average static structure of superhelical DNA (Klenin et al., 1995), this paper shows model calculations for the dynamics of structural changes in superhelical DNA that contains curved inserts.

A variety of models exist that describe the structure and internal dynamics of superhelical DNA (for a review, see Schlick, 1995). Of all these models, only simulations that include the solvent explicitly can calculate the dynamics from "first principles," that is, using only the known values for DNA bending and torsional persistence length, hydrodynamic radius, and electrostatic interactions. We have recently developed a numerical method to simulate the dynamics (and structure) of supercoiled DNA in aqueous solution based on Brownian dynamics (BD) (Chirico and Langowski, 1992, 1994). In this paper, we extend the previous model to simulate intrinsically curved sequences and electrostatic intramolecular interactions. For analyzing the trajectories calculated from the model, some structural and dynamic parameters are defined and the algorithms for their computation are described. In a third part, BD trajectories are analyzed in terms of these parameters and conclusions are drawn about the effect of curved sequences on the global structure of superhelical DNA and its dynamics.

METHODS

Brownian dynamics algorithm

The simulation of DNA motion in solution is performed by numerically integrating the Langevin equations (Ermak and McCammon, 1978; Fixman, 1978) for a model molecule. In the model (Chirico and Langowski, 1994) used here, the chain is described by a string of N beads with center-of-mass positions $\{\mathbf{r}_i\}_{i=1,N}$, and the rotational orientation of each bead relative to its equilibrium structure is described by a unit vector $\mathbf{f}$ fixed on the bead and perpendicular to the bead-to-bead direction, the bond direction (Allison et al., 1989). The discrete equations of motion in the solvent for the bead positions and for the torsion of the body fixed

Received for publication 7 March 1996 and in final form 16 May 1996.
Address reprint requests to Dr. Jörg Langowski, Abteilung Biophysik der Makromoleküle (0830), Deutsches Krebsforschungszentrum, Im Neuenheimer Feld 280, D-69120 Heidelberg, Germany. Tel.: 49-6221-423390; 49-6221-423391; joerg.langowski@dkfz-heidelberg.de.

0006-3495/96/08/955/17 $2.00

coordinates (bfc) systems associated with the beads are then (Dickinson et al., 1985)

$$\delta r_i(t) = \delta t \sum_j \underline{\mathbf{D}}_{ij}(t)\mathbf{F}_j(t)/(K_B T) + R_i(t)$$
$$\delta \phi_i(t) = \delta t D_r T_i(t)/(K_B T) + S_i(t), \quad (1)$$

where $\underline{\mathbf{D}}_{ij}$ is the hydrodynamic interaction matrix (see below), and $\mathbf{F}_j(t)$ and $T_i(t)$ are the forces and torques acting on the beads.

These equations are iterated with a time step δt, and the random displacements $R_i(t)$ and $S_i(t)$ are sampled from Gaussian distributions with the following momenta:

$$\langle R_i(t)\rangle = 0; \quad \langle R_i(t):R_j(t)\rangle = 2\delta t \underline{D}_{ij}(t)$$
$$\langle S_i(t)\rangle = 0; \quad \langle S_i(t)S_j(t)\rangle = 2\delta t D_r. \quad (2)$$

The new **f** vectors are obtained by summing to the old **f** vectors the so-called drift and twist displacements (Allison et al., 1989):

$$\mathbf{f}_i(t + \delta t) = \mathbf{f}_i(t) + \delta^{\text{twist}}\mathbf{f}_i(t) + \delta^{\text{drift}}\mathbf{f}_i(t)$$
$$= \mathbf{f}_i(t) + \delta\phi_i(t)\mathbf{v}_i(t) - \mathbf{u}_i(t)(\delta\mathbf{u}_i(t)\cdot\mathbf{f}_i(t)), \quad (3)$$

where the unit vectors $\mathbf{u}_i(t)$ and $\mathbf{v}_i(t)$ are defined as

$$\mathbf{u}_i(t) = (\mathbf{r}_{i+1}(t) - \mathbf{r}_i(t))/|\mathbf{r}_{i+1}(t) - \mathbf{r}_i(t)|$$
$$\mathbf{v}_i(t) = \mathbf{u}_i(t) \times \mathbf{f}_i(t). \quad (4)$$

The DNA molecules simulated here are covalently closed, and periodic boundary conditions have been assumed: $\mathbf{r}_{i+N} = \mathbf{r}_i$ and $\mathbf{f}_{i+N} = \mathbf{f}_i$. The $(3N \times 3N)$ $\underline{\mathbf{D}}_{ij}$ matrix in the first line of Eqs. 1 and 2 is the Rotne-Prager generalization of the Oseen tensor (Rotne and Prager, 1969). The rotational diffusion coefficient around the long axis of the DNA segment is $D_r = K_B T/(4\pi\eta a^2 b_0)$, where b_0 is the bond length, i.e., the bead-to-bead distance, and a is the bead radius.

The bending and torsional potentials are harmonic, as in Allison et al. (1989), with a different derivation of the corresponding forces (Chirico and Langowski, 1994). The longitudinal stiffness is taken into account by a harmonic stretching potential. The complete algorithm is thoroughly described by Chirico and Langowski (1994), and we report here only the parameters used for the simulation discussed in this work and some specific changes to the interaction potentials.

Each bond length $b_i = |\mathbf{r}_{i+1} - \mathbf{r}_i|$ is kept constant at $b_o = 12.736$ nm by means of a stretching potential corresponding to a variance $(\langle b_i^2\rangle - \langle b_i\rangle^2)^{0.5} = 0.008\ \langle b_i\rangle$ at the simulation temperature $T = 298$ K. The stretching potential is

$$U_s = \frac{K_B T}{2\delta^2} \sum_{i=0}^{N} (b_i - b_0)^2. \quad (5)$$

This stretching potential was chosen as a compromise between the length of the simulation time step and the deviation of the calculated DNA persistence length from the theoretical value (Chirico and Langowski, 1992).

We use nontouching beads (i.e., $a = 2.527$ nm), and the force constants were rescaled as described by Chirico and Langowski (1994). The bending and torsional potentials are

$$U_b = \frac{K_B T}{2\Psi^2} \sum_{i=0}^{N} (\beta_i - \beta_{0,i})^2 \quad (6)$$

$$U_t = \frac{K_B T}{2\xi^2} \sum_{i=0}^{N} (\alpha_i + \gamma_i)^2, \quad (7)$$

where $\{\alpha_i, \beta_i, \gamma_i\}_i$ are the Euler angles for rotating the body fixed coordinate system (bfc) of the ith bead into that of the $(i + 1)$th bead. ψ determines the variance of β and is related to A through $A = b_o K_B T/\Psi^2$.

The values for the bending and torsional rigidities are $A = 2 \cdot 10^{-19}$ erg cm and $C = 2.6 \cdot 10^{-19}$ erg cm. A is equivalent to a dynamic persistence length $P = 50$ nm, corresponding to the deviations of the chain axis from its equilibrium value due to thermal motion. Our calculations did not take into account the static persistence length, which corresponds to the deviation of the DNA helix axis from straight equilibrium due to sequence variation (Trifonov et al., 1987). Such variations are only considered for the formation of large permanent bends at a small number of defined positions in the molecule and are taken into account by the bending angles $\beta_{o,i}$.

The consensus value of the apparent persistence length is $P = 50$ nm (Hagerman, 1988). Recent work (Trifonov et al., 1987) estimates the dynamic contribution to 75 nm and the static one to 150 nm; therefore, our choice of A is a lower bound. The value of $C = 2.6 \cdot 10^{-19}$ erg cm corresponds to $\xi = 0.445$ in Eq. 6, because $C = b_o K_B T/\xi^2$. This value is an average of recently published determinations of C that span a range of $2.0 \cdot 10^{-19}$ erg cm $\leq C \leq 3.0 \cdot 10^{-19}$ erg cm.

The main difference from our previous work (Chirico and Langowski, 1994) is the introduction of a new potential function for describing permanent curvature. Nonzero equilibrium bending angles $\beta_{o,i}$ in Eq. 1 are introduced, together with a third potential energy function U_k, called hereafter "kink potential." U_k is meant to constrain the intrinsic curvature to a chosen plane in the bfc local system. The form assumed here

$$U_k = \frac{K_B T}{2\xi^2} \sum_{i=0}^{N} (\alpha_i - \alpha_{0,i})^2 \sin^2(\beta_{0,i}) \quad (8)$$

has already been used in the BD simulation of DNA fragments containing intrinsically curved sequences (Collini et al., 1995). Let us consider, for example, the case $\{\alpha_{0,i} = 0; \beta_{0,i} = B_0; i = 0, \ldots m\}$. With B_0 some constant value $\neq 0$, this part of the chain corresponds to a curved piece of DNA composed of m bonds in a plane. Clearly it is not required that all β_0 angles have the same constant value over the curved region. A helical structure, for example, is given by the case $\{\alpha_{0,i} = A_0; \beta_{0,i} = B_0; i = 0, \ldots m\}$, where B_0 and A_0 are some constant values $\neq 0$. The parameter ζ takes into account the fluctuations of the curved structure around equilibrium. We have arbitrarily chosen $\zeta = 0.1$ as a default value. This parameter by itself, not taking into account the torsional potential, would determine a variance $\sigma_\alpha = \zeta/\sin(\beta_0)$ of α at the curvature point. As an example, for bending angles $\beta_0 \cong 30°$ the corresponding rms value of α is $\cong 11°$. The forces and torques acting on the beads and the bfc systems are explicitly derived according to the procedure outlined in the appendix of Chirico and Langowski (1994).

A fourth potential describes intramolecular repulsion. These interactions, which had been simulated with a truncated Lennard-Jones potential in the previous paper (Chirico and Langowski, 1994), are mainly electrostatic and are now described in a Debye-Hückel approximation (Tanford, 1961). Modeling the bonds as thin rods and in analogy with the theory developed by Stigter (1977) for two infinitely long rods, the intramolecular force between two bonds is assumed to be

$$|F| = F_0 b_0^2 \exp(-d_{min}/\kappa)/(d_{min}^2 \text{sen } \phi), \qquad (9)$$

where d_{min} is the minimum distance between the two bonds, $\kappa = 3$ nm and sen $\phi = \sin(\phi)$, if $\phi > 0.01$; 0.01, if $\phi \leq 0.01$. The distribution of the force over the four beads involved is made on each bond through the lever rule with respect to the points corresponding to the minimum distance between the bonds. The force is repulsive and directed along the line joining the lever points. F_0 is assumed to be 3.12 $k_B T b_0$, which yields $|F| \approx k_B T b_0$ when $d_{min} \approx b_0/2 = 6.3$ nm. This effective helix diameter corresponds to an ionic strength of 0.1 M (Rybenkov et al., 1993), although the assumed screening length κ would correspond to $I = 0.01$ M. A more rigorous treatment of the electrostatic interactions (Hammermann et al., manuscript in preparation) also confirms this correspondence.

We had previously used a hard-core repulsive potential to take into account the excluded-volume interactions (Chirico and Langowski, 1994). The qualitative conclusions from those calculations for DNAs without bent inserts, as far as the dynamics of superhelix formation are concerned, were the same as in the present work. As shown by Rybenkov et al. (1993), a hard-core repulsive potential gives the correct dependence of DNA knotting probabilities on ionic strength for $[Na^+] \leq 1$ M. At high ionic strengths around 1 M, however, the form of the electrostatic potential at close distances might influence the chain dynamics. A systematic investigation of ionic effects on the superhelix dynamics through simulations and dynamic light scattering measurements is currently under way.

The forces entering the beads' equations of motion (Eqs. 1 and 2) are the sum of the stretching, bending, torsional, electrostatic, and kink forces. The stretching and torsional forces are the same in Eqs. A3 and A27 of Chirico and Langowski (1994). The bending forces are a simple generalization of those reported in the cited reference (Eq. A6 of Chirico and Langowski, 1994); the β_i angles in front of the second term of the equation are changed into $(\beta_i - \beta_{0,i})$. The electrostatic forces are given by summing Eq. 9 over all bond pairs, and the "kink" forces are derived from the kink potential U_k as described in the Appendix. The torques are the sum of 1) the torques derived in the appendix of Chirico and Langowski (1994) and 2) the torques derived from the kink potential U_k as described in the Appendix of this paper.

The BD algorithm starts from an initial configuration (see below) and computes at each step the translational and rotational displacements via Eqs. 1–4. The trajectories were calculated over $1–10 \cdot 10^6$ steps with an integration time step of 193.2 ps. Initial configurations used in this work were 1) a flat circle, 2) a straight plectonemic structure, or 3) the final configuration of a Monte Carlo simulation obtained by a procedure similar to that described by Klenin et al. (1995). In the first case the deficit linking number ΔLk is initially uniformly distributed over the twisting angles. For the second and third choices, the writhing number of the conformation is computed and the twist $Tw = \Delta Lk - Wr$ is uniformly distributed over the chain.

Molecular structure and dynamics

In this section some structural and dynamic paramters are defined and the algorithms for their computation are described.

Characterization of the structure

The BD simulation describes the behavior of molecules under the influence of internal, external, and solvent interaction forces. We show in the following that the configuration of a circular DNA under torsional stress evolves quite rapidly into a metastable entangled state from which it is difficult to escape, and final equilibration may be very slow. To assess the time scales of the internal dynamics and the extent of equilibration, we have to devise structural parameters that characterize the intramolecular motions and follow their dynamics to see when a "substantial rearrangement" has occurred in the molecule. A supercoiled DNA has well-defined structures like "loops" and "branches," and at least parts of the molecule adopt a plectonemic structure. It is therefore plausible to look for the location, size, and dynamics of loops and branches. We summarize in the following the definition of some structural quantities that will be used to characterize the structure and dynamics of the simulated supercoiled DNA.

Antipode plot

As suggested by Sprous et al. (1995), a slowly varying structural quantity is the so-called antipode distance. The distance

$$da_i = |\mathbf{r}_{i+N/2} - \mathbf{r}_i| \tag{10}$$

between monomers i and $i + N/2$, where N is the total number of monomers, is computed along the chain and plotted against i. For a perfect plectonemic DNA with two loops, this plot has a sinusoidal shape with large peak-to-peak variation. If the DNA changes its plectonemic structure appreciably, by extruding other loops or by changing the position of the existing ones through slithering of the chain, the positions or the number of the peaks in the antipode plot will change during the simulation. With increasing simulation time, the average antipode plot will approach a flat line where the periodic changes have been smoothed out.

Local density

One important feature of a supercoiled DNA structure is that parts of the chain that are distant along the sequence approach each other in space. Each monomer may therefore have many nonadjacent nearest neighbors. We define a local neighbor density ρ_i as the number of monomers whose distance from the ith monomer is less than a radius r_o. Here this quantity has been assumed to be $r_o = 12$ nm, similar to the superhelix diameter observed in cryoelectron microscopy (Bednar et al., 1994).

Nearest-neighbors matrix

In the determination of many structural quantities it will be important to know the nearest neighbors of a monomer. As before, the jth monomer is a nearest neighbor of the ith monomer if $|\mathbf{r}_i - \mathbf{r}_j| < r_o$. During the computation of the local density, a matrix nn[N][N] and a vector in[N] are built as follows:

in[i] = the number of nearest neighbors of the ith monomer

nn[j] = the index of the jth nearest neighbor of the ith monomer; $j = 1, \ldots, \text{in}[i]$.

Local writhe

Supercoiled DNA obeys the well-known topological theorem (White, 1989)

$$Lk = Tw + Wr, \tag{11}$$

which states that the linking number, Lk, of the two polynucleotide strands equals the sum of the twist (Tw), which is the number of DNA helix turns around its local axis, and the writhe (Wr), which is a measure of the degree of coiling of the DNA helix axis in space. Wr is equal to the number of self-crossings of the helix axis in a two-dimensional projection, averaged over all orientations. One possible way to compute Wr is via the Gaussian integral (White, 1989). For our discrete model of N monomers we use the approximate expression

$$Wr = \frac{1}{4\pi} \sum_{i=0}^{N} \sum_{k=0}^{N} (\mathbf{r}_{i+1} - \mathbf{r}_i) \times (\mathbf{r}_{k+1} - \mathbf{r}_k) \cdot \frac{(\mathbf{r}_k - \mathbf{r}_i)}{|\mathbf{r}_k - \mathbf{r}_i|^3}, \tag{12}$$

where circular boundary conditions are used, i.e., $\mathbf{r}_{i+N} = \mathbf{r}_i$.

If we restrict the sum in Eq. 8 to two parts of the molecule that are crossing each other in a planar projection, the resulting integral is approximately ± 1, the sign depending on the direction of the crossing. This comes from the fact that the vector product $(\mathbf{r}_{i+1} - \mathbf{r}_i) \times (\mathbf{r}_{j+1} - \mathbf{r}_j)$ is approximately parallel to the $\mathbf{r}_{i,j}$ vector joining two points of the two molecular moieties. We can therefore detect whether two parts of the molecule of equal length $2m$, centered at segments I and J, make a turn of a plectonemic superhelix by computing the local writhe:

$$Wr(I,K,m) = \frac{1}{4\pi} \sum_{i=I-m}^{I+m} \sum_{k=K-m}^{K+m} (\mathbf{r}_{i+1} - \mathbf{r}_i) \times (\mathbf{r}_{k+1} - \mathbf{r}_k) \cdot \frac{(\mathbf{r}_k - \mathbf{r}_i)}{|\mathbf{r}_k - \mathbf{r}_i|^3}. \tag{13}$$

Care must be taken in the choice of the summation length m, as discussed later.

Plectonemic percentage and diameter

A plectonemic or interwound region of the DNA molecule is defined as a region where two portions of the chain are intertwined. For a suitable choice of r_0, the number of nearest neighbors in[i] of monomer i in a plectonemic region is expected to be >0. Moreover, it may be expected that the ith monomer and its nearest neighbors are part of the same interwound region.

Let us assume that there is a sequence of monomers $\{i - 1, i, i + 1\}$, and the condition nb(i, k) is true if monomer k is a nearest neighbor of monomer i. We then use the definition that the monomer i belongs to a plectonemic region if nb(i, k), nb($k - 1$, $i + 1$) and nb($k + 1$, $i - 1$) are true at the same time (this also implies that the two interwound strands are running in opposite directions). The plectonemic percentage is the percentage of the monomers satisfying this definition. The indices of the monomers that belong to a particular plectonemic region of length j_{sup} are stored in a vector isup[k] ($k = 1, \ldots, j_{sup}$).

The average plectonemic diameter D_p is defined as the average distance between each of the monomers belonging to plectonemic regions and its corresponding nearest neigh-

bors. This definition is different from one used elsewhere (Vologodskii et al., 1992), where the superhelix diameter $\langle D \rangle$ is taken as the minimum distance between a monomer and the rest of the molecule (avoiding some immediately adjacent monomers), averaged over all monomers. This last quantity can be computed for any configuration but can be substantially different from the plectonemic diameter D_p, which describes more closely the actual superhelix diameter but obviously cannot be defined on noninterwound structures.

Position of a loop

The loop detection algorithm uses a combination of several criteria which has proved very efficient for DNA lengths of several kilobases. It is based on the computation of the nearest-neighbors matrix (nn), omitting some adjacent monomers (6 left and 6 right) from the calculation. In this case the tip of the loop corresponds to a region where no nearest neighbours are detected, because the loop conformation is expected to be rather open locally.

The basic algorithm consists in first detecting the positions where in[i] = 0, i.e., where no nearest neighbors have been detected. Obviously this algorithm cannot work as it is (imagine a flat circle where in[i] = 0 over the whole chain!), and some cross-checks are needed.

When a continuous region of the chain is found where in[i] = 0, the index, i, of the monomer in the center of this region is considered as a tentative loop position. The ith monomer is retained as the position of a loop if the two following conditions are met.

1) The local writhing number $Wr(i,i,m)$ is computed for $m = 10$ to $m = 1$, and an integer L_S is found such that $|Wr(i,i,L_S)| > 0.5$ and $|Wr(i,i,L_S - 1)| < 0.5$. L_S is taken as the size of the loop. The purpose of this last condition can be understood by considering that the local writhing number is ~0 in the close vicinity of the loop tip because the chain is almost flat.

2) The length of the interwound arm associated with the loop is checked to avoid the interpretation of minor extrusions of the DNA chain as a loop. A loop arm is imagined as a plectonemic region adjacent to the loop, and its length L_A is defined as the number of monomers in a plectonemic region within a distance $2L_S$ from the ith monomer. The tentative loop position indicated by condition 1) is retained if L_A is greater than 4 monomers (here ~50 nm).

Characterization of the dynamics

The dynamics of a long flexible macromolecule such as supercoiled DNA have a wide spectrum. Our primary aim in this work is to characterize quantitatively the slowest internal dynamics, particularly relative motions of distant parts of the molecule that may be important for long-range intramolecular interactions.

Slithering motion

We define the slithering movement of the ith monomer as the component of its motion tangent to the chain at $\mathbf{r}_i$:

$$\delta s_i(t) = (\mathbf{r}_{i+1}(t) - \mathbf{r}_{i-1}(t)) \cdot \delta\mathbf{r}_i(t)/|\mathbf{r}_{i+1}(t) - \mathbf{r}_{i-1}(t)|. \quad (14)$$

A slithering trajectory $s_i(t)$ is constructed by summing up $\delta s_i(t)$ during the BD simulation. Locally, this motion is a one-dimensional random walk; we therefore compute the correlation function

$$C_{s,i}(t) = \langle (s_i(t) - s_i(0))^2 \rangle = 2D_s(i)t \quad (15)$$

and obtain $D_s(i)$, the "slithering diffusion coefficient" of the ith monomer.

Antipode distance correlation

According to Sprous et al. (1995), the antipode distance da_i for a particular pair of monomers (i, $i + N/2$) (Eq. 10) can be computed during a simulation, and its fluctuations can be quantified through a correlation function:

$$C_{a,i}(t) = \langle da_i(t) da_i(0) \rangle_t. \quad (16)$$

The expected behavior for this function is a composite exponential decay.

Diffusion coefficients

Rigid body computation

The hydrodynamics of a rigid molecule in solution can be described by its translational and rotational diffusion coefficients, which can also be experimentally determined. We compute the diffusion coefficients of a particular configuration according to Garcia de la Torre et al. (Garcia de la Torre and Bloomfield, 1977), based on the theory developed by Brenner (1967). For a configuration composed of N beads, the friction matrices for translation and rotation and for their coupling are computed from the inverse $\underline{\mathbf{S}}$ of the $3N \times 3N$ supermatrix $\underline{\mathbf{Q}}$, whose 3×3 blocks are

$$\underline{\mathbf{Q}}_{i,j} = \delta_{i,j}\underline{\mathbf{I}} + (1 - \delta_{i,j})\zeta_i\underline{\mathbf{T}}_{i,j}. \quad (17)$$

Here $\underline{\mathbf{T}}$ and $\underline{\mathbf{I}}$ are the Rotne-Prager (1969) and the unit tensors. $\underline{\mathbf{S}}^{-1}$ is computed by a Gauss-Seidel method (Garcia de la Torre and Bloomfield, 1977), and a 6×6 friction matrix $\underline{\Xi}$ is built as a linear composition of the 3×3 submatrices of $\underline{\mathbf{S}}^{-1}$. The translation and rotation diffusion matrices are obtained from the 3×3 blocks of $k_BT\underline{\Xi}^{-1}$, and their eigenvalues are the three translational and rotational coefficients. The trace of the translational diffusion matrix is the translational diffusion coefficient D_t. A full description of the algorithm is given in the section "Computational procedure" in the cited reference (Garcia de la Torre and Bloomfield, 1977). The program based on this algorithm has been tested on the hydrodynamic coefficients of rigid and bent rods (Collini et al., 1995).

Center-of-mass correlation

A second independent way of computing D_t is through the center-of-mass displacement of a three-dimensional random walk:

$$\langle|\mathbf{R}_{cm}(t) - \mathbf{R}_{cm}(0)|^2\rangle = 6D_t t, \quad (18)$$

where $\mathbf{R}_{cm}(t)$ is the position of the center of mass of the molecule at time t.

RESULTS

Six trajectories were computed over 1 ms, starting from three different initial conformations as listed in the Methods section with and without a 100° permanent bend. The bend was simulated by setting the β_0 angles between four consecutive segments to 25°. Eight more trajectories were computed, up to a total time of 0.2 ms. Taken together, the simulations took more than 6 months of cpu time on a 150-MHz SGI Indy R4400. Thus, although the results presented here are representative for the typical dynamic behavior of a DNA superhelix, better statistics can be expected from parallelizing the simulation algorithms. This work is currently under way in our group.

Writhing number evolution

The writhing number may be taken as a first indicator of the overall shape of the DNA molecule. When starting from a flat circle with high torsional stress ($\Delta Lk = Tw = -10$, $Wr = 0$), the writhing number changes in about 10 μs toward a value close to equilibrium (~ -5). During the first microsecond, the circle assumes a locally toroidal form; thermal fluctuations then induce the nucleation of end loops of interwound regions, and in general a branched interwound conformation is formed in this first phase. However, the dominant equilibrium form for an 1870-bp DNA is an unbranched interwound structure (Boles et al., 1990). The relaxation toward this form increases the writhe only by a small amount and is much slower than the initial relaxation, as shown in Fig. 1 *c*.

When the simulation is initiated from a straight interwound structure, which is much less torsionally stressed, the writhing number relaxes again during the first 10 μs from its initial value of -8 toward its equilibrium of approx. -6.5 (Fig. 1 *b*). When the starting configuration is sampled from a Monte Carlo simulation, the writhing number does not show any indication of an initial fast relaxation (Fig. 1 *a*).

In all three cases, the equilibrium value of Wr is $\cong -6.5 \pm 0.5$. No difference is detected in either the equilibrium value or its fluctuation when the permanent bend is introduced.

Diffusion coefficients

The translational diffusion coefficient can be computed from each configuration in the trajectory by a rigid-body

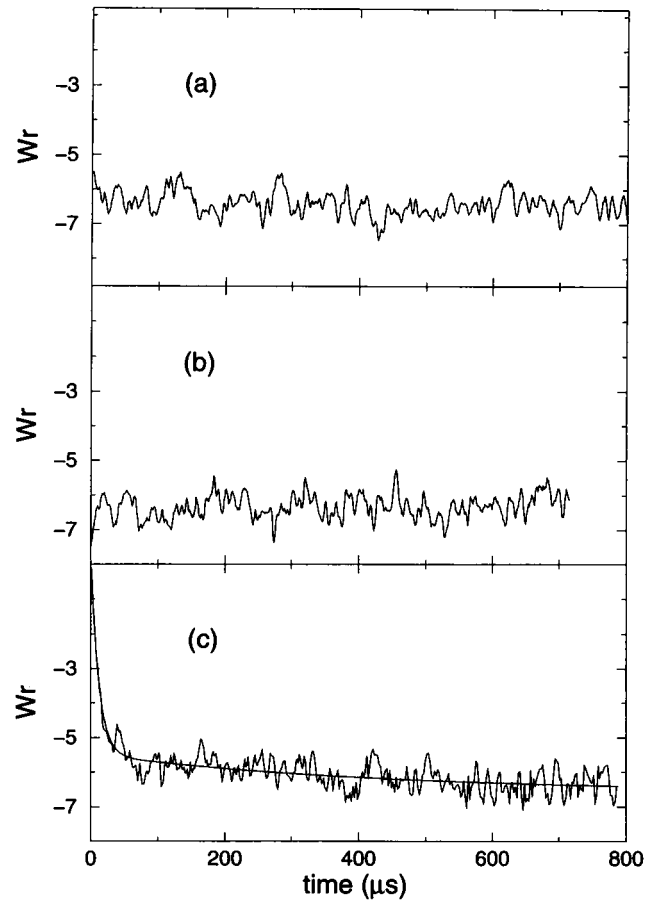

FIGURE 1 Time evolution of the writhing number for the simulations starting from a Monte Carlo sampled configuration (*a*), a straight interwound (*b*), and a flat circle (*c*). The lower curve was fitted by a sum of two decaying exponentials (see text).

treatment (Garcia de la Torre and Bloomfield, 1977) or derived by evaluating the slope of the center-of-mass correlation function (Eq. 18). In Fig. 2 this correlation function is plotted against time for some trajectories, showing a fairly linear behavior up to 10 μs. The diffusion coefficients evaluated by this method are reported in Table 1 together with those obtained from the average translational diffusion coefficient computed by the rigid-body treatment over each configuration in the trajectory. The values obtained through the rigid-body treatment are all very close to $(6.85 \pm 0.2) \cdot 10^{-12}$ m^2/s. The slopes of the center of mass correlation function lead to D_t values with larger uncertainty and with an average $D_t = (7.2 \pm 0.7) \cdot 10^{-12}$ m^2/s, in reasonable agreement with the rigid-body result. The rather high discrepancy between the center-of-mass and rigid-body results for the circle (no bend) trajectory might stem from the fact that this particular trajectory is still quite far from global equilibrium and there is a systematic variation in the global conformation.

The rotational diffusion coefficients are evaluated with the rigid-body treatment only. In general, two of the three eigenvalues (D_{r1}, D_{r2}) are close to each other and signifi-

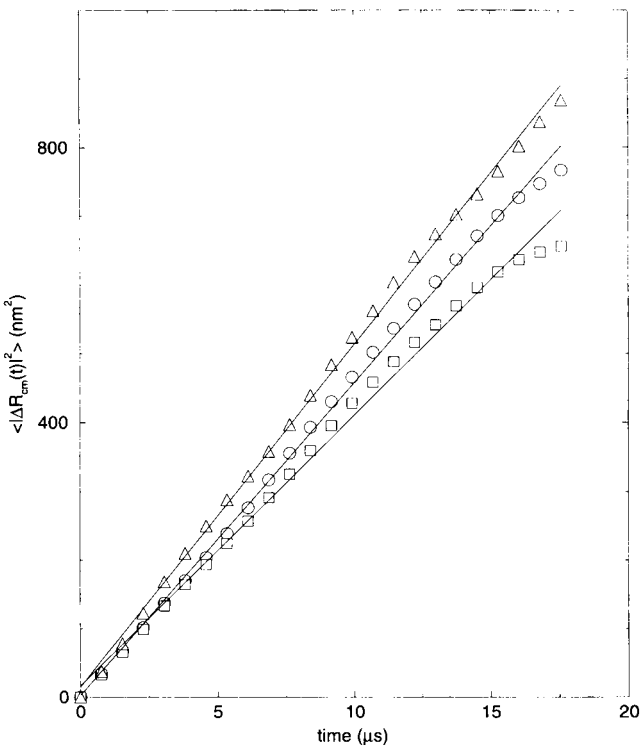

FIGURE 2 Center of mass correlation functions for three trajectories starting from a flat circle (△), straight interwound (○), and Monte Carlo sampled initial configurations (□).

cantly smaller than the third one (D_{r3}), indicating an approximately cylindrical symmetry. The distributions of the ratio $|D_{r1} - D_{r2}|/D_{r3}$ for different trajectories have their maximum at ~0.07 with a tail up to 0.2 (data not shown). Although the rotational asymmetry is not extreme (see below), we may define an average tumbling rotational diffusion coefficient $R_{tumb} = (D_{r1} + D_{r2})/2$ and a spinning rotational diffusion coefficient $R_{spin} = D_{r3}$ for the purpose of comparing different trajectories and parts of the same trajectory.

The average values of R_{tumb} and R_{spin} are reported in Table 2 for the six trajectories studied here. The trajectories starting from a flat circle—even though the initial 100 μs were omitted from the computation—show R_{tumb} and R_{spin} values closer to each other than the corresponding values for the sampled conformation. This result reflects the more globular conformation for the trajectory starting from the circle, which has not reached the equilibrium that is more closely approximated by the trajectories starting from the straight interwound and from the Monte Carlo conformation.

The average values over all six trajectories are R_{tumb} = 2.6 ± 0.3 kHz and R_{spin} = 5.8 ± 0.5 kHz.

Superhelix diameter

The diameter of the interwound parts of the chain was computed as described in the Methods section. The distribution functions for two trajectories starting from straight interwound configurations are plotted in Fig. 3. These distributions have a clear maximum with an approximately Gaussian shape (see the solid line in Fig. 3). The values of the average and the fluctuation of the plectonemic diameter D_p are shown in Table 3.

Plectonemic content

The definition of the interwound parts of the chain is detailed in the Methods section. The distribution functions for the plectonemic content are plotted in Fig. 4 for the six trajectories presented here. Their averages are given in Table 4.

Contrary to the case of diffusion coefficients, writhing number, and superhelix diameter, the values of the average of the plectonemic percentage depend substantially upon the type of the initial conformation, but again are relatively insensitive to the presence of curved inserts. An appreciable difference is found between the simulations starting from flat circles and those starting from less strained configurations (interwound or Monte Carlo). In these last cases slightly lower values are found for the cases with a permanent bend.

The distribution functions are monomodal, except for the simulation run from a Monte Carlo starting configuration in the presence of a bend, where two peaks were found (Fig. 4 *a*).

Radius of gyration

The trajectory started from a Monte Carlo sampled conformation in the absence of a permanent bend shows a bimodal distribution for R_g (data not shown). For the other cases, the distribution of R_g is well described by a Gaussian curve. The average values $\langle R_g \rangle$ are reported in Table 5.

Writhing autocorrelation function

The writhing number is a global structural quantity, and its temporal fluctuations are related to the global dynamics of the superhelix structure. To assess the effect of a bend on the internal dynamics of the DNA, we have analyzed the autocorrelation function of the writhing number, defined as

$$G_{Wr}(\tau) = \frac{\langle Wr(t)Wr(t+\tau)\rangle}{\langle Wr(t)^2\rangle}, \qquad (19)$$

where $Wr(t)$ is the instantaneous writhe of the conformation at time t, and $\langle\rangle$ indicates the time average. The average was taken after an initial relaxation period of 200 μs over the remaining trajectory. A single exponential function was then fitted to $G_{Wr}(\tau)$, and its relaxation time was used to characterize the internal motions. Table 6 shows that the internal dynamics of the superhelix are indeed influenced by local structural differences: the initial decay of the correlation function for the writhing number is slower when a

TABLE 1 Translational diffusion coefficients*

Trajectory type (no bend)	D_t center-of-mass	D_t rigid body	Trajectory type (+ bend)	D_t center-of-mass	D_t rigid body
Circle	8.2 ± 0.4	6.9 ± 0.4	Circle	7.2 ± 0.3	6.85 ± 0.4
Interwound	6.4 ± 0.6	6.7 ± 0.35	Interwound	6.4 ± 0.6	6.6 ± 0.4
Monte Carlo	7.2 ± 0.2	7.0 ± 0.3	Monte Carlo	7.9 ± 0.6	6.7 ± 0.3

* In 10^{-12} m^2/s units. Errors reported are the uncertainties of the parameters in the least-squares fit.

permanent bend is present. The corresponding relaxation times are on the order of 2–3 μs (Table 6).

Kremer et al. (1993) observed a decrease in the amplitude of fast internal motions of superhelical DNAs with permanently bent inserts. There it was hypothesized from the results of Monte Carlo simulations (Klenin et al., 1995; Kremer et al., 1993) that the localization of the end loop by the bend limits certain types of internal motions where the bend has to be stretched. The finding that writhe fluctuations are slower in the presence of the bend is in agreement with this hypothesis.

Kinetics of loop migration

No intrisic curvature

The first part of the trajectory in Fig. 5 was started from a flat circle in the absence of permanent bends (at t = 450 μs a bend was inserted; see below). As already shown by Chirico and Langowski (1994), during the first 10 μs the torsional stress and thermal fluctuations drive parts of the chain out of the plane (Fig. 5 b) These positions then act as nucleation point for loops. After approximately 50 μs, some loops are absorbed into others and three or four loops remain. During the first 450 μs we never observed fewer than three loops, the positions of which shifted by ~10 monomers (i.e., 130 nm) over 200–300 μs.

When starting from a straight interwound configuration (Figs. 6 and 8), the molecule's initial regular structure is distorted by thermal motion, but only after approximately 300 μs do we see a substantial rearrangement in the position of the loops: the two original end loops that were at positions 0 and 25 have shifted to 8 and 26, and a third short loop is formed at position 45. After reformation of a two-loop structure, a three-loop structure is formed again at 575 μs. Thus, the dynamics of structural rearrangement are characterized by the formation and disappearance of loops on a time scale of several 100 μs. Similar behavior is found if the output of a Monte Carlo simulation is used as the starting configuration (Figs. 7 and 8).

TABLE 2 Rotational diffusion coefficients

Starting configuration	$\lvert D_{r1} - D_{r2}\rvert/D_{r3}$	R_{tumb} (kHz)	R_{spin} (kHz)
Circle, no bend	.075 ± .04	3.1 ± 0.6	5 ± 0.9
Circle + bend	.065 ± .03	2.8 ± 0.6	5.5 ± 1.1
Interwound, no bend	.06 ± .05	2.3 ± 0.6	5.8 ± 1.1
Interwound + bend	.08 ± .05	2.3 ± 0.6	5.8 ± 1.1
Monte-Carlo, no bend	.085 ± .06	2.2 ± 0.6	6.4 ± 1.2
Monte-Carlo + bend	.06 ± .035	2.8 ± 0.5	6.4 ± 1.3

Insertion of an intrinsically curved sequence

In three simulations, we introduced a 100° planar permanent bend during the course of the trajectory by setting the equilibrium bending angles $\beta_{o,i} = 25°$ and $\alpha_{o,i} = 0°$ for four consecutive segments $i = m - 1 \ldots m + 2$, where m is defined as the center of the bend. In the first example (Fig. 8, *bottom*), the bend was introduced at position 3 at t = 450 μs. The loop at position 7 which was already present is

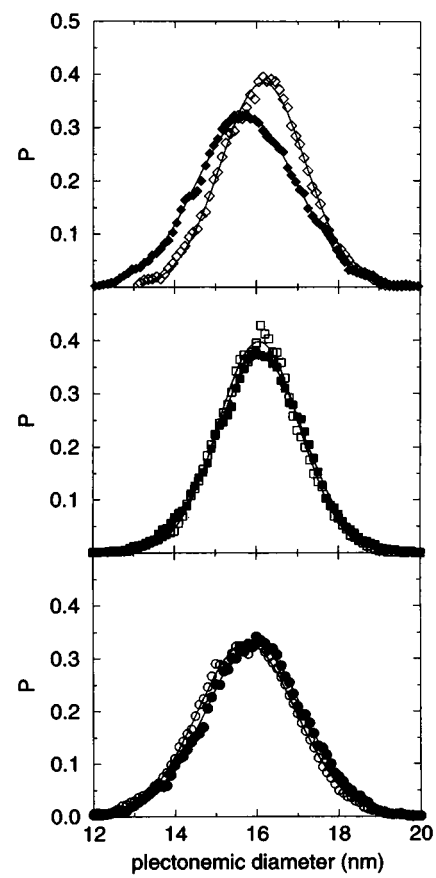

FIGURE 3 Distribution functions of the superhelix diameter for the trajectories starting from a flat circular configuration (*bottom*), a straight interwound configuration (*middle*) and a Monte Carlo sampled configuration (*top*). Open and filled symbols refer to the simulations run in absence and in presence of a bend. Solid lines are best-fit Gaussian curves of the data.

TABLE 3 Average plectonemic diameter

Starting conf.	$\langle D_p \rangle$ (nm)	Starting conf.	$\langle D_p \rangle$ (nm)
Circle, no bend	15.7 ± 1.7	Circle + bend	16.0 ± 1.7
Interwound, no bend	16.0 ± 1.0	Interwound + bend	16.0 ± 1.5
MC, no bend	16.2 ± 1.5	MC + bend	15.7 ± 1.7

TABLE 4 Average plectonemic percentage

Starting conf.	% plectonemic	Starting conf.	% plectonemic
Circle, no bend	29 ± 10	Circle + bend	29 ± 10
Interwound, no bend	45 ± 12	Interwound + bend	40 ± 12
MC, no bend	45 ± 14	MC + bend	28 ± 9

stabilized and shifted to position 3 within approximately 50 μs. Otherwise, in the following 500 μs the structure stays in a three-branch configuration.

In the second example (Fig. 9, *bottom*) the simulation starts from a straight interwound structure containing a 100° bend which is centered at position 25 and at t = 200 μs moved to position 15. In the first 200 μs loops remain at positions 0 and 25, and a branch starts to extrude after ~100 μs at position 40. After the shift of the bend to position 15, a new loop appears there, and the loop in position 25 is slowly (over 400 μs) coalescing with the new one. At the same time the loop at position 2 drifts to position 40.

In the third example, again the permanent bend is introduced almost exactly between two existing loops (Fig. 9, *top*). Here the simulation started from an initial Monte Carlo configuration where two loops were present in 10 and 30, and the permanent bend was introduced at position 22 at t = 0 μs. At 300 μs a loop is detected at position 20. During the duration of this very long trajectory, the configuration stays three-looped most of the time, and although the bend at position 20 clearly leads to the formation of a loop, the structure never changes completely into a straight form with loops at positions 20 and 45.

In summary, structural changes induced by a bend seem to occur on a time scale of 300–800 μs when the bend is far away from the initial loop position, and in about 50 μs when the distance over which the loop has to move is only on the order of four segments (140 bp).

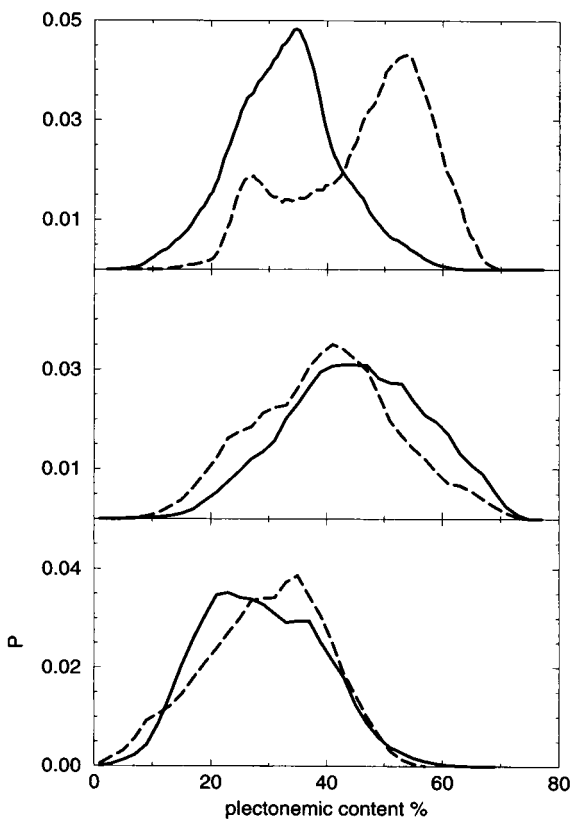

FIGURE 4 Distribution functions of the plectonemic percentage for the trajectories starting from a flat circle (*bottom*), a straight interwound configuration (*middle*), and a Monte Carlo sampled configuration (*top*). The solid and dashed lines refer, respectively, to the simulations run in the absence and in the presence of a bend.

DISCUSSION

Convergence of the trajectory

An important issue in a dynamics simulation of a biopolymer is to establish whether the trajectory has reached equilibrium. For reliable computations of physical quantities and comparison with experimental results one needs a trajectory that samples a representative part of the configuration space.

The kinetics of global rearrangement can be quantified by the "antipode plot" proposed by Sprous et al. (1996) as explained in the Methods section. When a substantial displacement of the loop tips has occurred, the shape of the plot of da_i versus the monomer index i is expected to change significantly, and the average of the antipode distance $\langle da_i \rangle$ over a long simulation would be independent of the index i. In Fig. 10, the antipode plot, $\langle da_i \rangle$ versus i, is shown for a 2.1-ms trajectory starting from a Monte Carlo sampled configuration. A maximum is always found at the positions where the initial two loops are resident, i.e., positions ≅ 10 and 30, as can be seen from the loop positions plot in Fig. 9 (*top*). The amplitude of the antipode plot (difference between maximum and minimum) can be taken as a measure of the kinetics of convergence toward equilibrium. As the inset in Fig. 10 shows, there is an initial relaxation in the 0.5-ms range, but the amplitude seems to take much longer to relax fully to zero.

An "equilibrium dynamic state" cannot be expected before the initial configuration has visited a sufficient number of

TABLE 5 Radius of gyration

Starting conf.	R_g (nm)	Starting conf.	R_g (nm)
Circle, no bend	39.0 ± 3.6	Circle + bend	41 ± 4
Interwound, no bend	45.3 ± 5.7	Interwound + bend	46 ± 6
MC, no bend	46.6 ± 5.6	MC + bend	39 ± 4

TABLE 6 Writhing number relaxation times

Starting conf.	τ_{wr} (μs)	Starting conf.	τ_{wr} (μs)
Circle, no bend	0.7 ± 0.3	Circle + bend	1.8 ± 0.4
Interwound, no bend	2.7 ± 0.4	Interwound + bend	4 ± 0.4
MC, no bend	1.5 ± 0.3	MC + bend	2.2 ± 0.4

different possible states and therefore has substantially changed the structure (i.e., position of the maxima and minima) of its antipode plot. From the loop position plots (Figs. 8 and 9) it is evident that global rearrangements of an 1870-bp superhelix take place on a scale of 0.5 ms; thus 1–2 ms is only a fraction of the time that is needed to reach a state of dynamic equilibrium. We estimate that the simulation time needed for reliable statistical averages would be at least in the 10-ms range, i.e., an average over 20 independent configurations. Because of the cpu time needed (this study took several months of continuous calculation on an SGI Indy R4400), the simulations reported here could not be extended further; however, many of the dynamic features and time scales reported very likely hold also for the equilibrium state. For instance, when a permanent bend is displaced by 10 monomers, i.e., 130 nm (as in Fig. 9, *botttom*), the structure of a major part of the molecule changes in only ~50 μs: the loop at 25 splits into two loops at 17 and 30. Other global rearrangements may take longer, as can be judged by following the time evolution of the tumbling rotational diffusion coefficient (Fig. 11). A new two-looped conformation is reached only 0.5 ms after the displacement of the bend.

In the case of an initially flat circle ($\Delta Lk = Tw$), representing an out-of-equilibrium state with large torsional stress, the writhe reaches 70% of its final value $\langle Wr \rangle$ in approximately 15 μs (Fig. 1 *c*). Only after ~0.4–0.5 ms has Wr reached its equilibrium value (cf. the two-exponential relaxation indicated by the continuous line in Fig. 1). This slow relaxation may be due to the extremely out-of-equilibrium starting configuration.

For a straight interwound starting configuration (Fig. 1 *b*), the writhing is initially only slightly overestimated ($Wr \approx -8$) and reaches an apparent equilibrium in only 50 μs, after which the writhe fluctuates around $Wr \approx -6.5$; no slow relaxation process is apparent. In the time dependence of other structural parameters, such as the tumbling and spinning rotational diffusion coefficients, the initial fast relaxation ($\leq$50 μs) is even more pronounced. Still, other major conformational changes do take place on slower time scales (see the change of R_{tumb} from $\cong$ 1.5 kHz to $\cong$ 4 kHz at times $\cong$ 200–300 μs), although no evidence of this transition can be detected from the writhe plot. A similar behavior is seen when the starting configuration is generated by a Monte Carlo procedure.

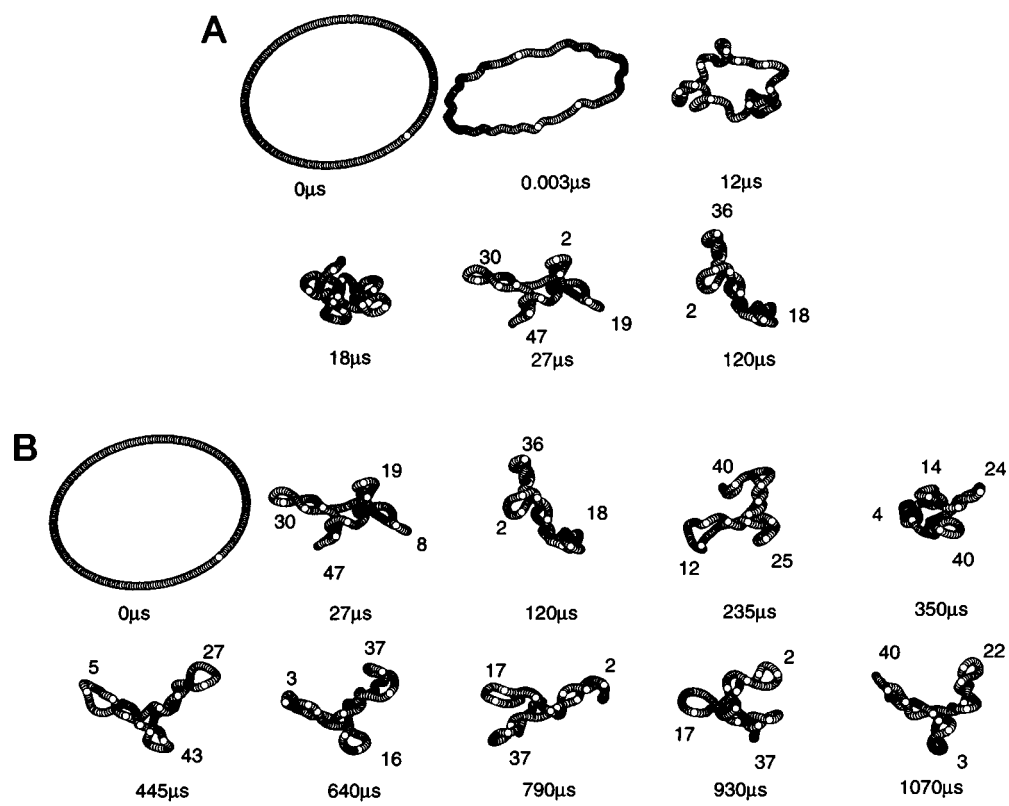

FIGURE 5 Configurations from the trajectory started from a flat circle in the absence of permanent bends. Simulation times are marked next to the configuration, and loop positions close to the loop tips. (*a*) The first 120 μs; (*b*) the whole evolution up to 1 ms. At 0.45 ms a bend was introduced at position 3; it is marked with filled spheres in the plot.

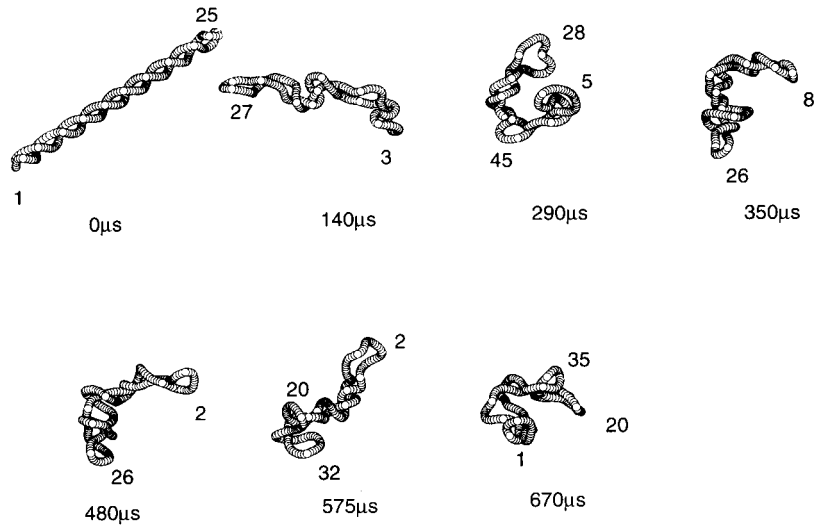

FIGURE 6 Configurations from the trajectory started from a straight interwound conformation in the absence of permanent bends. Simulation times are marked next to the configuration, and loop positions close to the loop tips.

Dependence on the initial conformation

As described above, the equilibration time for the conformation of 1870 bp superhelical DNA is on the order of several hundred microseconds; thus, the simulation result is expected to depend on the initial conformation for shorter trajectories. However, most of the structural parameters evaluated in the Results section are not very sensitive to the initial conformation after the first 100 μs. The average writhe is very similar for all six trajectories discussed above (cf. Fig. 1) and therefore does not depend appreciably either on the initial conformation or on the presence of a permanent bend. The same behavior is found for the superhelix diameter and the loop size.

On the other hand, the plectonemic percentage does show a substantial variation over the different types of initial conformations, reflecting the different number of loops found in the trajectories. This is particularly evident when comparing the trajectory starting from a flat circle with the others. Other structural parameters, such as the tumbling and spinning diffusion coefficients, are remarkably similar for the two trajectories starting from a straight interwound and from a Monte Carlo sampled conformation, but differ substantially between these two trajectories and the one starting from a flat circle.

Again, this shows the presence of long relaxation processes that may take up to several milliseconds. A flat circle is in fact an extremely out-of-equilibrium state that seems to take more than the 1.2 ms simulated here to reach a state of "dynamic equilibrium." The existence of one such state cannot be firmly stated here, although the similarity of the structural characteristics evaluated after 1 ms of simulation, for the trajectories starting from almost "equilibrated" though fairly different states (interwound and Monte Carlo), supports such a hypothesis.

Comparison with experimental data

Boles et al. (1990) collected structural information on pBR322 derivatives by electron microscopy (EM). The smallest plasmid studied there (pJB3.5d) was 3480 bp long, i.e., twice as large as in our simulations. The EM studies

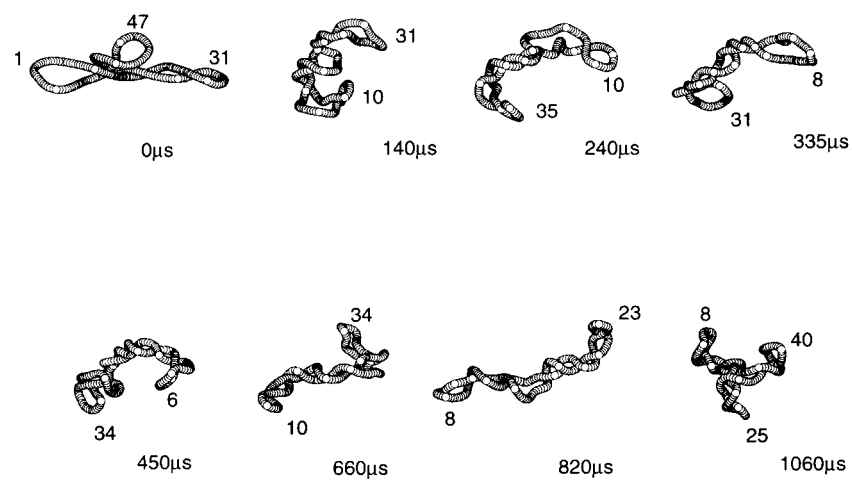

FIGURE 7 Some configurations are shown from the trajectory started from a Monte Carlo sampled conformation in the absence of permanent bends. Simulation times are marked next to the configuration, and loop positions close to the loop tips.

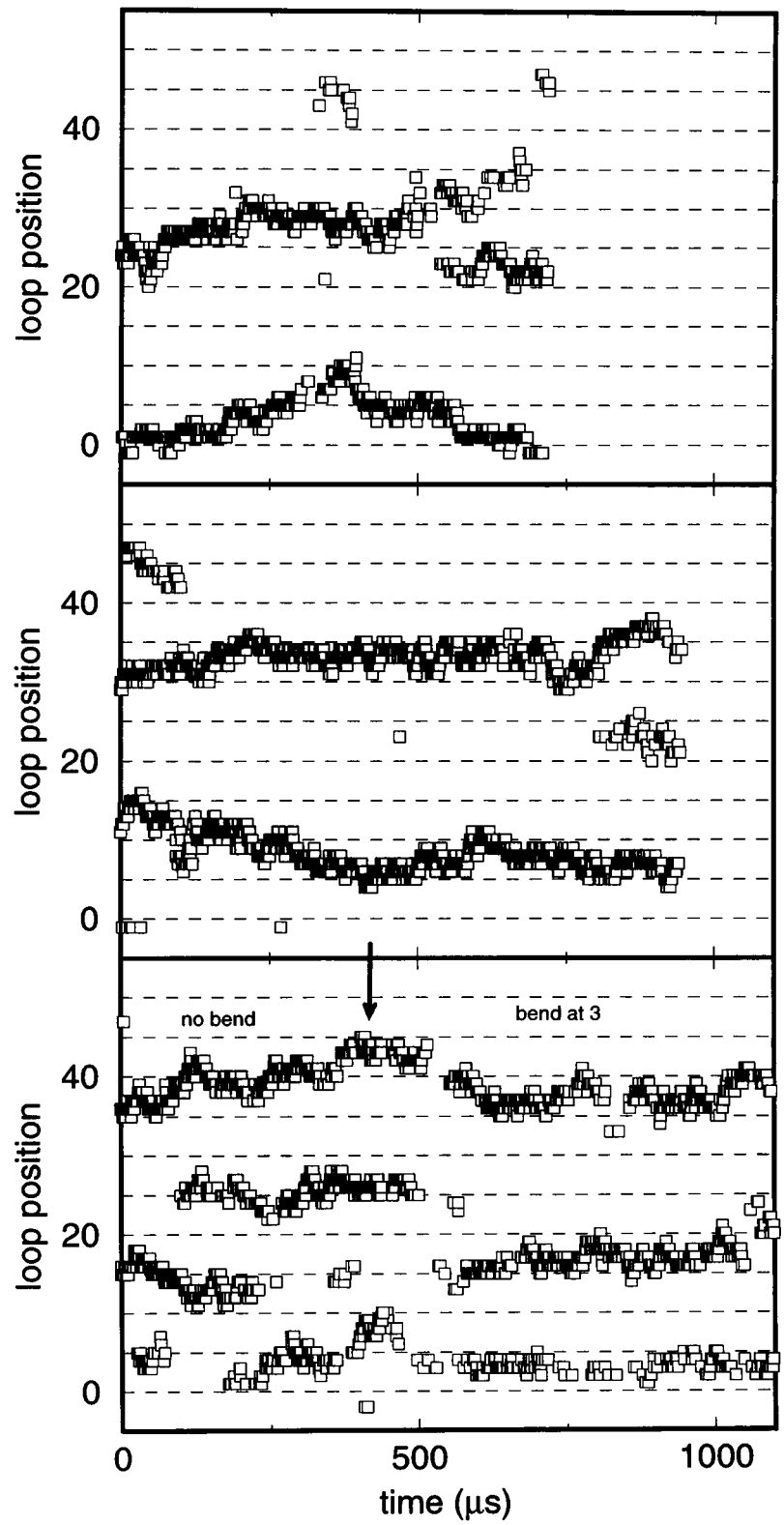

FIGURE 8 Time evolution of the loop positions for the trajectories starting from a flat circle (*bottom*), Monte Carlo sampled (*middle*), and straight interwound (*top*) configurations. After 0.45 ms a permanent bend in position 3 was introduced in the simulation starting from a flat circle, as indicated by the arrow in the bottom panel.

were conducted at 10 mM ionic strength; here we approximate the electrostatic interactions through a repulsive potential that has the same effective diameter d_{eff} ($U(d_{eff}) = kT$) as measured for DNA at 0.1 M salt, i.e., $d_{eff} = 6.3$ nm.

The average superhelical density σ, the plectonemic diameter D_p, and the plectonemic percentage r_p found here, $\sigma = -0.65 \pm 0.05$, $D_p = 16 \pm 2$ nm, $r_p = 40 \pm 12\%$, computed over the four trajectories corresponding to initial interwound

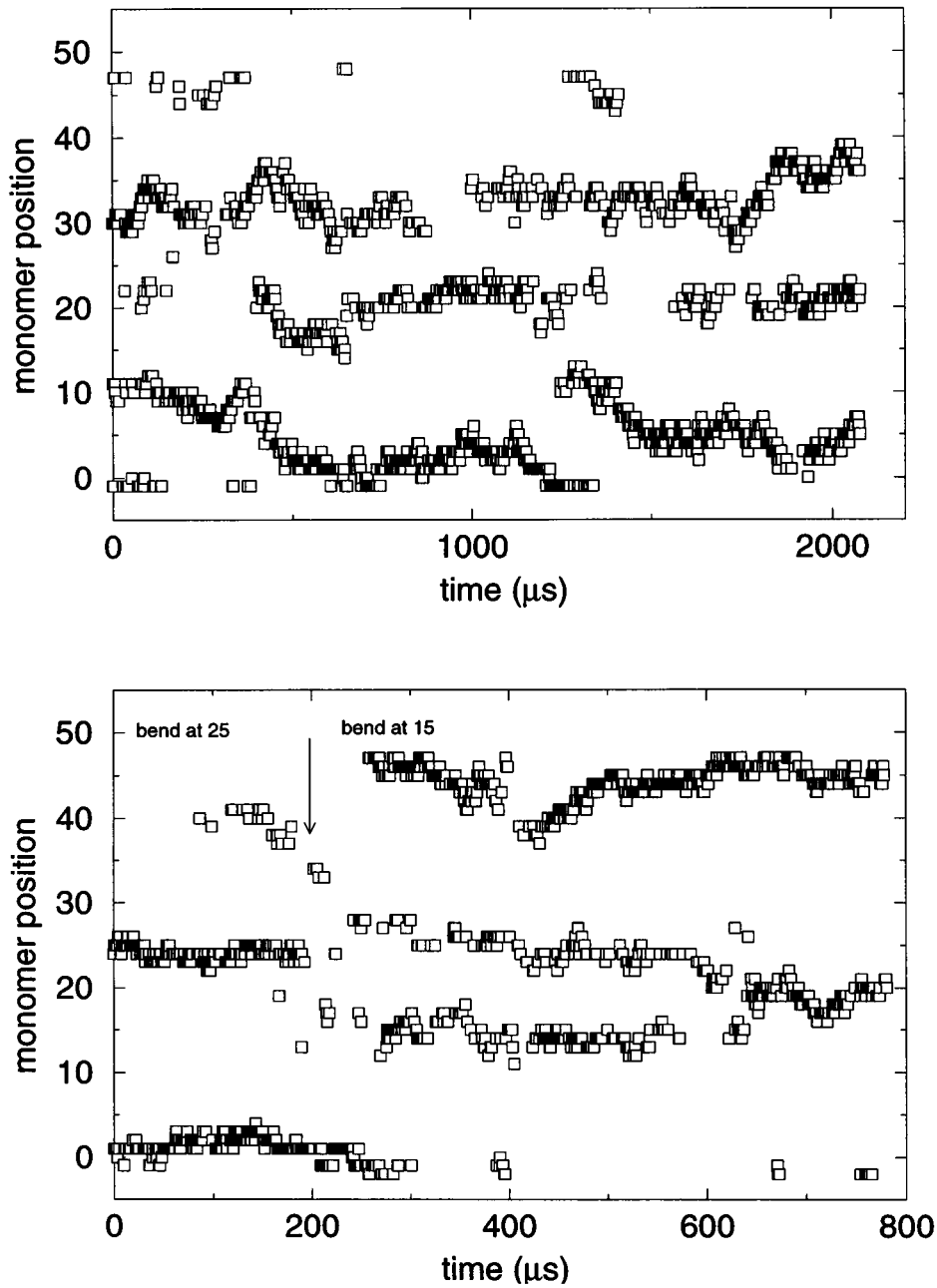

FIGURE 9 Time evolution of the loop positions for the trajectories starting from straight interwound (*top*) and Monte Carlo sampled (*bottom*) configurations. In the top panel a bend was set at position 20, and in the bottom panel a permanent bend initially at position 25 is moved to position 15 after 0.2 ms.

and Monte Carlo configurations, agree reasonably well with the experimental findings of Boles et al. (1990): $\sigma = 0.72 \pm 0.03$, $D_p = 14 \pm 1.2$ nm, and $r_p = 35$–40% (see Eq. 12 and figures 11 and 12 of Boles et al., 1990).

The diffusion coefficient of an 1868-bp DNA plasmid at native superhelical density has been determined recently (Steinmaier et al., manuscript in preparation): $D_t = (7.0 \pm 0.5)\ 10^{-12}$ m^2/s. The translational and rotational diffusion coefficients for 1870-bp plasmids can also be predicted by extrapolating the logarithmic laws reported by Langowski and Giesen (1989): $D_t = D_t(M_0) \cdot (M/M_0)^{-0.6 \pm 0.1}$ and $R = R(M_0) \cdot (M/M_0)^{-2.7 \pm 0.3}$. By taking the most recent experimental determinations of D_t and R for pUC18 plasmid (2686 bp), $D_t = (5.5 \pm 0.3)\ 10^{-12}$ m^2/s, and $R_{tumb} = (1.1 \pm 0.1)$ kHz (Chirico and Baldini, 1996), one predicts for a 1870-bp plasmid that $D_t = (6.8 \pm 0.24)\ 10^{-12}$ m^2/s and $R_{tumb} = (2.9 \pm 0.3)$ kHz. Both the experimental D_t and the extrapolated D_t and R values agree very well with the averages over all of the trajectories reported here, $D_t = (6.9 \pm 0.2)\ 10^{-12}$ m^2/s and $R_{tumb} = (2.6 \pm 0.3)$ kHz.

Is there "local slithering"?

Different types of trajectory evolution for the above choices of initial configurations can be seen in the loop position plots (Figs. 8 and 9). General features of the loop position evolution are 1) slithering (like in Fig. 8, *middle*, for the loop originally

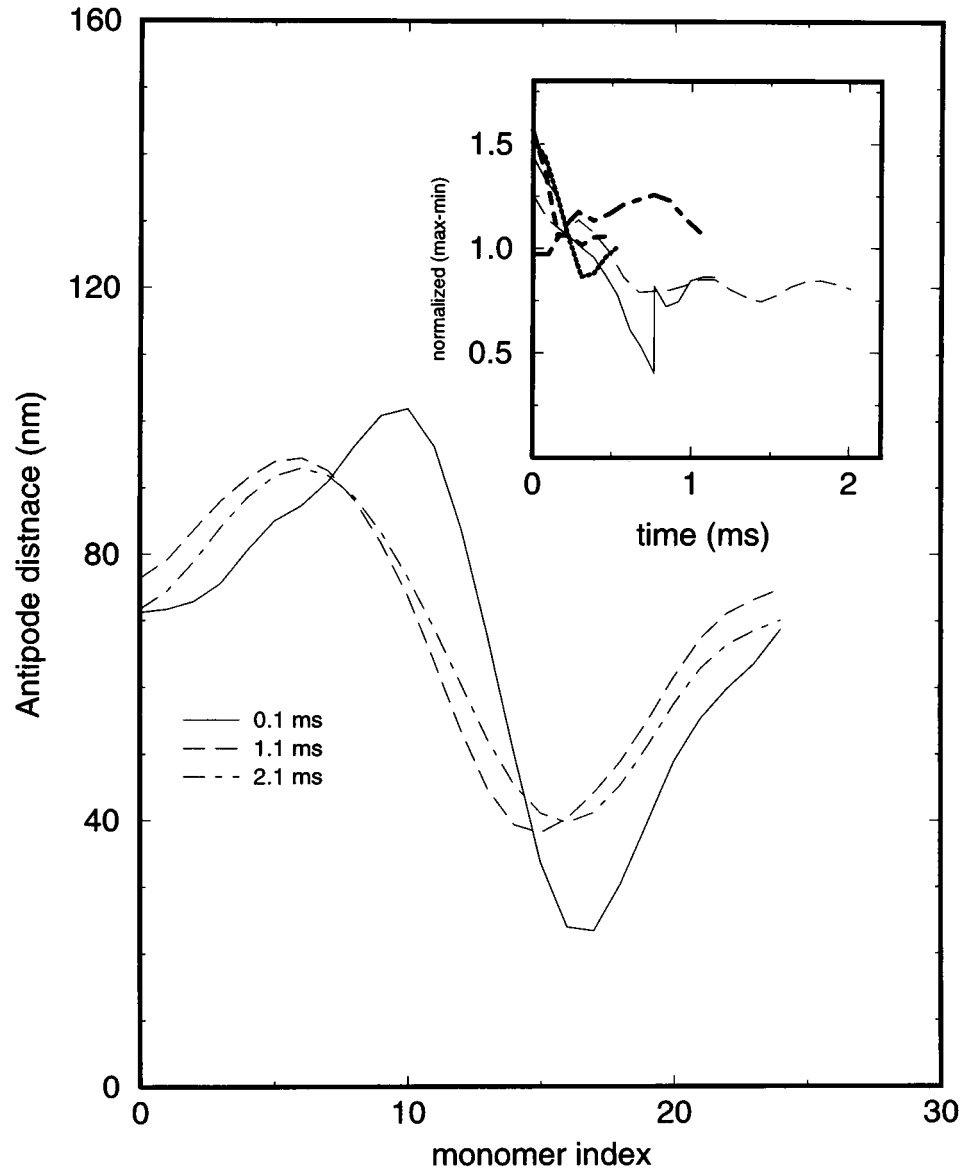

FIGURE 10 Antipode distance averaged over a trajectory starting from a Monte Carlo sampled configuration with a bend at position 20 after 0.1, 1.1, and 2.1 ms of simulation time. The maximum variation of the antipode distance over the chain normalized to the mean antipode distance is shown in the inset for the simulations discussed in the text.

at position 15), 2) the formation or disappearance of a loop (like at positions 15 and 25 in the first 0.5 ms in Fig. 8, *bottom*), and 3) the splitting of one loop into two loops (as for the loop in position 25 in Fig. 9, *bottom*, after 200 μs, or the loop at position 20 after 1.3 ms in Fig. 9, *top*).

As can be seen from Figs. 8 and 9, the extent of slithering, i.e., the continuous random migration of the loop position with time, typically is at most 10–15 monomer units (i.e., 130–200 nm) over 1 ms. In Fig. 8 (*middle*) (Monte Carlo sampled initial conformation), the loop in position 15 is found in position 8 after ~500 μs. In the simulation run from an initial interwound configuration (Fig. 8, *top*), the loop in position 0 diffuses to position 10 in ~400 μs and then moves back to 0 during the next 400 μs. In the bottom panel of Fig. 8, for the simulation run from a flat circular initial configuration, the loop in position 35 diffuses up to position 45 in the first 450 μs. This last case is also characterized by the formation and disapperance of several loops in the first 500 μs when no intrinsically curved sequence has been introduced.

The conclusion is that although over short distances slithering motion is found, no evidence is seen for a large-scale structural rearrangement due to slithering. Major rearrangements occur through the formation and disappearance of loops.

The effect of a curved insertion on the conformation

The introduction of a bend comprising 8% of the contour length can have quite different effects on the configuration and on the evolution of the loop positions versus time. When a loop was present near the position of the introduced bend, the DNA conformation was stabilized. This effect is more evident in the case when the starting configuration is a flat circle. In the first part of the evolution of the chain the loops are slithering (loop

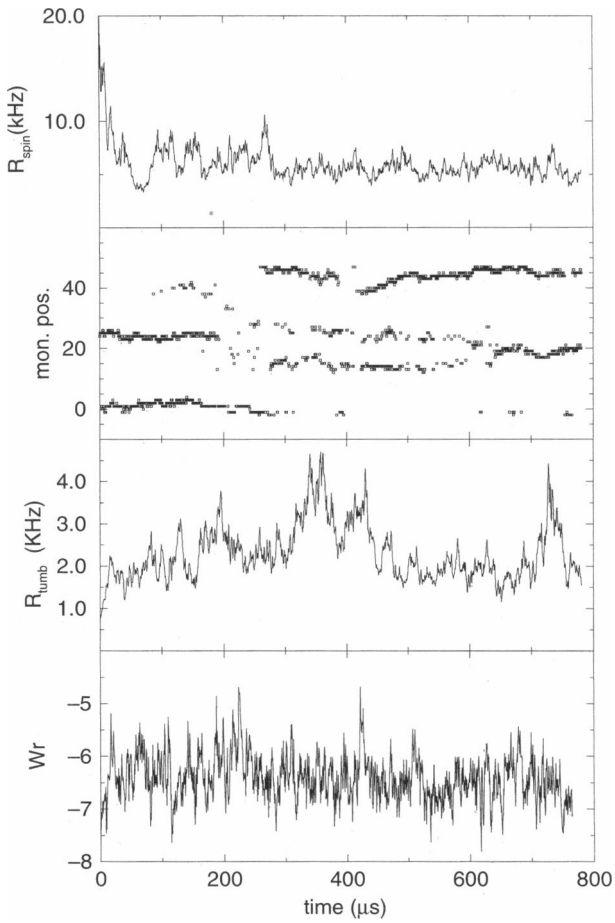

FIGURE 11 Spinning R_{spin} and tumbling R_{tumb} rotational diffusion coefficients, writhing number Wr, and loop positions for a trajectory starting from a straight interwound chain versus time. A permanent bend is first placed at position 25 and moved to position 15 after 0.2 ms.

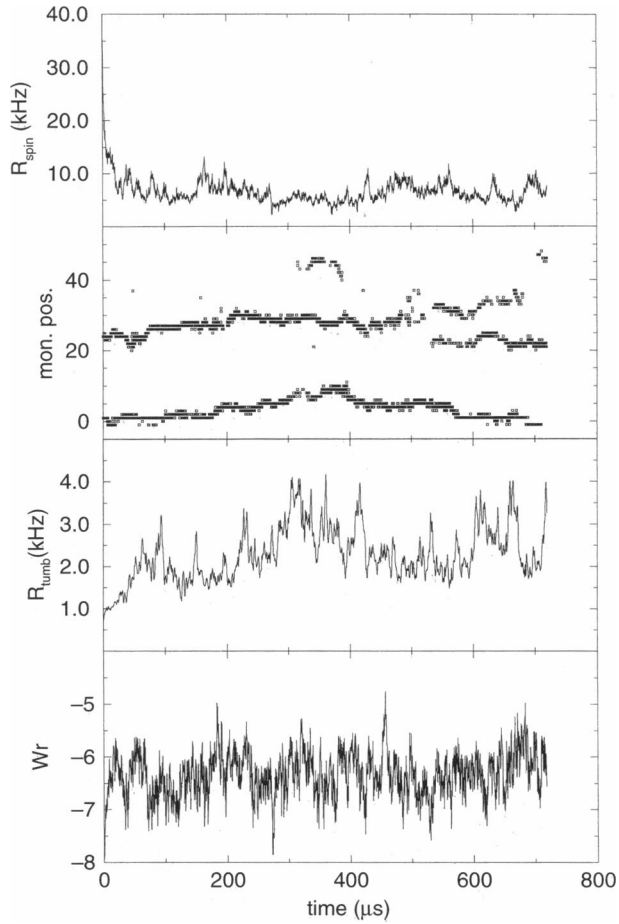

FIGURE 12 Spinning R_{spin} and tumbling R_{tumb} rotational diffusion coefficients, writhing number Wr, and loop positions for a trajectory starting from a straight interwound chain versus time without permanent bend.

in ≅ 37), and appearing or disappearing (loops in ≅ 5, 15, and 25). The introduction of the intrinsically curved sequence in position ≅ 3 greatly stabilizes the loop in the close vicinity of the bend, and it also affects parts of the molecules that are within ≅ 150 nm of the point of the introduction of the curved sequence, as can be seen by the shift in position of the loops at positions 25 and 45.

The structural change induced by the bend can take place over a rather long time. This is evident from Fig. 9 (*bottom*) (initial interwound configuration), where the shift of the bend from 15 to 25 induces the sudden appearance of a loop in the new position of the bend (position 15), but the loop that was present at position 25 takes ~500 μs to disappear. Furthermore, the loop at position 1 shifts to position 40 (resp. −10, due to the chain closure) after the displacement of the curved sequence. Again, the curved sequence induces changes in rather distant parts of the molecule (~300 nm).

Local slithering diffusion of the monomers

A slithering diffusion coefficient $D_s(i)$ can be obtained from the slope of $C_{si}(t)$ versus time (Eq. 15); this plot is linear to good approximation (data not shown). $D_s(i)$ gives an estimate of the average monomer displacement along the chain axis and around an equilibrium position.

In Fig. 13 the values of $D_s(i)$ are plotted versus the monomer index and in parallel with the loop positions (Fig. 13, *bottom*). A clear correlation between the loop position and the value of $D_s(i)$ is found everywhere, and no substantially different behavior can be found for the loops corresponding (or stabilized) to a permanent bend. The slithering Brownian motion of a monomer along the chain corresponds to a fluctuation around its equilibrium position and not to steady motion along the chain. The above results show that the interwound portions of the chain suffer fewer position fluctuations along the helix axis than the tip of the loops. Incidentally, the average value $\langle D_s \rangle = 30 \times 10^{-12}$ m^2/s is similar to the slope of the fast relaxation rate of the dynamic light scattering autocorrelation functions at high scattering vectors (Langowski, 1987).

CONCLUSIONS

The evolution of the structure of an 1870-bp circular DNA with $Lk = -10$ (i.e., superhelical density $\sigma = -0.056$) has been followed for 1–2 ms. Three different types of intial

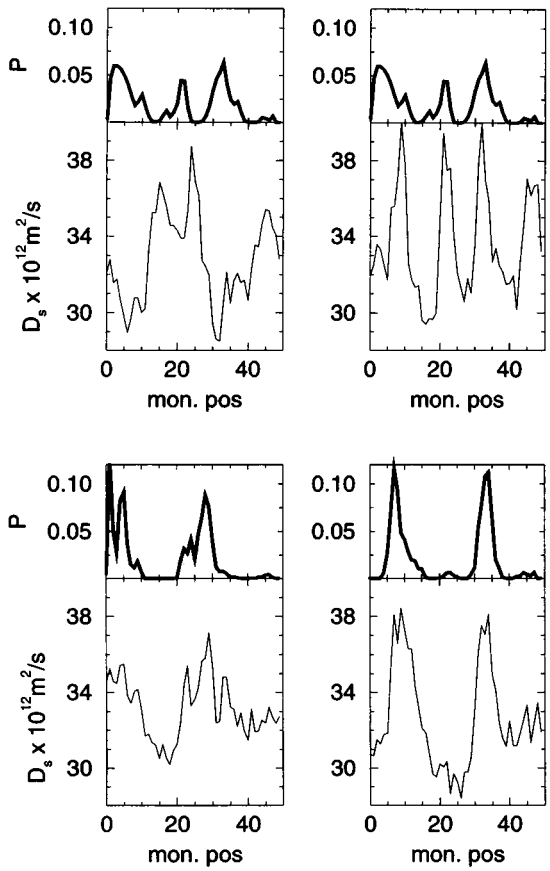

FIGURE 13 The slithering diffusion coefficients D_s (*thin lines*) and the probability of appearance of a loop (*thick lines*) versus the position along the chain (i.e., the monomer index) for the trajectories starting (*a*) from a straight interwound configuration without and with (*b*) a bend, (*c*) from a Monte Carlo sampled configuration without and with (*d*) a bend, as described in the text.

configuration were used: flat circle, straight interwound, and Monte Carlo sampled configurations. Several structural parameters (radius of gyration, superhelix diameter, plectonemic content, diffusion coefficients) have been averaged over all trajectories, with only minor differences between the three starting configurations.

We see a certain local "slithering" of chain segments along the DNA contour, which is significantly faster at the loop tip than in other parts of the chain. However, major rearrangements of the structure, such as changes between three- and two-looped forms or displacements of loops over longer distances, do not occur by slithering, but by the formation/destruction of loops. The characteristic time for such processes is on the order of 0.5 ms, with variations over at least an order of magnitude.

The introduction of a permanent bend (amounting to 8% of the contour length) in a position along the chain close to an existing loop seems to induce a stabilization of the structure. However, if the permanent bend is introduced far from any existing loop, it may take 0.5 to 1 ms for the structure to change according to this external perturbation. The insertion of a bend also affects the global chain dynamics, as seen in the autocorrelation function of the writhe. The effect of a permanent bend on the internal motions of superhelical DNA has first been observed experimentally by Kremer et al. (1993).

The simulation time of 1–2 ms that could be achieved here is only a fraction of the time necessary for the molecule to visit a substantial portion of the configuration space, and therefore some of our results must be interpreted on a qualitative basis. Statistically sound predictions of relaxation times, arm lengths, etc., will have to be based on much larger ensembles that currently can only be obtained on parallel computers. Our results, however, show the possibility of simulating the time evolution of the structure of a DNA molecule of relatively large size and the response of this molecule to external perturbations, e.g., a bend induced by a DNA-protein interaction.

APPENDIX: FORCES AND TORQUES FROM THE KINK POTENTIAL

The forces and torques are derived from the kink potential by the general method outlined by Chirico and Langowski (1994). The change in U_k upon an infinitesimal change in the Euler angles is given by

$$\delta U_k = -\frac{K_B T}{\zeta^2} \sum_{i=0}^{N} \frac{(\alpha_i - \alpha_{0,i})}{\sin(\alpha_i)} \sin^2(\beta_i)\delta\cos(\alpha_i) \left(\frac{\sin^2(\beta_{0,i})}{\sin^2(\beta_i)}\right). \tag{A1}$$

By substituting Eqs. 16 and 18 of Chirico and Langowski (1994) for the change in $\cos(\alpha_i)$ into Eq. A1, one finds

$$\delta U_k = -\frac{KBT}{\zeta^2} \sum_{i=0}^{N} \left(\frac{\delta \mathbf{r}_{i+2}}{|\mathbf{b}_{i+1}|} \cdot \mathbf{h}_i - \frac{\delta \mathbf{r}_{i+1}}{|\mathbf{b}_{i+1}|}\right.$$

$$\left. \cdot \mathbf{h}_i - \cos(\beta_i)\frac{\delta \mathbf{r}_{i+1}}{|\mathbf{b}_i|} \cdot \mathbf{h}_i + \cos(\beta_i)\frac{\delta \mathbf{r}_i}{|\mathbf{b}_i|} \cdot \mathbf{h}_i\right)\left(\frac{\sin^2(\beta_{0,i})}{\sin^2(\beta_i)}\right) \tag{A2}$$

$$-\frac{K_B T}{\zeta^2} \sum_{i=0}^{N} \delta\phi_i(\alpha_i - \alpha_{i,o})\sin^2(\beta_i),$$

where

$$\mathbf{h}_i = \frac{(\alpha_i - \alpha_{0,i})}{\sin(\alpha_i)} \mathbf{A}_i, \tag{A3}$$

$|\mathbf{b}_i|$ is the ith bond length and

$$\mathbf{A}_i = \sin(\beta_i)\mathbf{f}_i + \cos(\beta_i)\cos(\alpha_i)\mathbf{u}_i - \cos(\alpha_i)\mathbf{u}_{i+1}. \tag{A4}$$

By making the simplifying assumption

$$\frac{\sin^2(\beta_{0,i})}{\sin^2(\beta_i)} \cong 1 \tag{A5}$$

in first part of Eq. A2, and by simple index algebra, one can write

$$\delta U_k = -\sum_{i=0}^{N} \mathbf{F}_i \cdot \delta \mathbf{r}_i - \sum_{i=0}^{N} \delta\phi_i |T_i|, \tag{A6}$$

where

$$\mathbf{F}_i = \frac{K_B T}{\zeta^2}\left(\frac{\mathbf{h}_{i-2}}{|\mathbf{b}_{i-1}|} - \frac{\mathbf{h}_{i-1}}{|\mathbf{b}_i|} - \frac{\mathbf{h}_{i-1}}{|\mathbf{b}_{i-1}|}\cos(\beta_{i-1}) + \frac{\mathbf{h}_i}{|\mathbf{b}_i|}\cos(\beta_i)\right) \tag{A7}$$

and

$$T_i = \frac{K_B T}{\zeta^2}(\alpha_i - \alpha_{i,0})\sin^2(\beta_{i,0}). \tag{A8}$$

We thank Katalin Tóth and Gero Wedemann for critical reading of the manuscript.

Part of this work has been supported by grants of the Deutsche Forschungsgemeinschaft (La 500/4-2) and NATO (CRG 910239) to JL.

REFERENCES

Allison, S. A., R. Austin, and M. Hogan. 1989. Bending and twisting dynamics of short linear DNAs—analysis of the triplet anisotropy decay of a 209-base pair fragment by Brownian simulation. *J. Chem. Phys.* 90:3843–3854.

Bednar, J., P. Furrer, A. Stasiak, J. Dubochet, E. H. Egelman, and A. D. Bates. 1994. The twist, writhe and overall shape of superhelical DNA change during counterion-induced transition from a loosely to a tightly interwound superhelix. Possible implications for DNA structure in vivo. *J. Mol. Biol.* 235:825–847.

Boles, T. C., J. H. White, and N. R. Cozzarelli. 1990. Structure of plectonemically supercoiled DNA. *J. Mol. Biol.* 213:931–951.

Borowiec, J. A., L. Zhang, S. Sasse-Dwight, and J. D. Gralla. 1987. DNA supercoiling promotes formation of a bent repression loop in lac DNA. *J. Mol. Biol.* 196:101–111.

Brenner, H. 1967. Coupling between the translational and rotational Brownian motions of rigid particles of arbitrary shape. *J. Colloid Interface Sci.* 23:361–407.

Chirico, G., and G. Baldini. 1996. Rotational diffusion and internal motions of circular DNA: polarized photon correlation spectroscopy. *J. Chem. Phys.* 104:6009–6019.

Chirico, G., and J. Langowski. 1992. Calculating hydrodynamic properties of DNA through a second-order Brownian dynamics algorithm. *Macromolecules.* 25:769–775.

Chirico, G., and J. Langowski. 1994. Kinetics of DNA supercoiling studied by Brownian dynamics simulation. *Biopolymers.* 34:415–433.

Collini, M., G. Chirico, G. Baldini, and M. E. Bianchi. 1995. Conformation of short DNA fragments by modulated fluorescence polarization anisotropy. *Biopolymers.* 36:211–225.

Dickinson, E., S. A. Allison, and J. A. McCammon. 1985. *J. Chem. Soc. Faraday Trans. 2.* 81:591–601.

Ermak, D. L., and J. A. McCammon. 1978. Brownian dynamics with hydrodynamic interactions. *J. Chem. Phys.* 69:1352–1359.

Fixman, M. 1978. Simulation of polymer dynamics. I. General theory. *J. Chem. Phys.* 69:1527–1537.

Garcia de la Torre, J., and V. A. Bloomfield. 1977. Hydrodynamic properties of macromolecular complexes. I. Translation. *Biopolymers.* 16: 1747–1763.

Hagerman, P. J. 1988. Flexibility of DNA. *Annu. Rev. Biophys. Biophys. Chem.* 17:265–286.

Klenin, K., M. D. Frank-Kamenetskii, and J. Langowski. 1995. Modulation of intramolecular interactions in superhelical DNA by curved sequences. A Monte-Carlo simulation study. *Biophys. J.* 68:81–88.

Kremer, W., K. Klenin, S. Diekmann, and J. Langowski. 1993. DNA curvature influences the internal motion of superhelical DNA. *EMBO J.* 12:4407–4412.

Langowski, J. 1987. Salt effects on internal motions of superhelical and linear pUC8 DNA. *Biophys. Chem.* 27:263–271.

Langowski, J., and U. Giesen. 1989. Configurational and dynamic properties of different length superhelical DNAs measured by dynamic light scattering. *Biophys. Chem.* 34:9–18.

Langowski, J., W. K. Olson, S. C. Pedersen, I. Tobias, T. P. Westcott, and Y. Yang. 1996. DNA supercoiling, localized bending and thermal fluctuations. *Trends Biochem. Sci.* 21:50.

Laundon, C. H., and J. D. Griffith. 1988. Curved helix segments can uniquely orient the topology of supertwisted DNA. *Cell.* 52:545–549.

Rotne, J., and S. Prager. 1969. Variational treatment of hydrodynamic interaction in polymers. *J. Chem. Phys.* 50:4831–4837.

Rybenkov, V. V., N. R. Cozzarelli, and A. V. Vologodskii. 1993. Probability of DNA knotting and the effective diameter of the DNA double helix. *Proc. Natl. Acad. Sci. USA.* 90:5307–5311.

Schlick, T. 1995. Modeling superhelical DNA: recent analytical and dynamic approaches. *Curr. Opin. Struct. Biol.* 5:245–262.

Sprous, D., and S. C. Harvey. 1996. Action at a distance in supercoiled DNA: effect of sequence on slither, branching, and intramolecular concentration. *Biophys. J.* 68:A101.

Stigter, D. 1977. Interactions of highly charged colloidal cylinders with applications to double stranded DNA. *Biopolymers.* 16:1435–1448.

Tanford, C. 1961. Physical Chemistry of Macromolecules. Wiley, New York.

ten Heggeler-Bordier, B., W. Wahli, M. Adrian, A. Stasiak, and J. Dubochet. 1992. The apical localization of transcribing RNA polymerases on supercoiled DNA prevents their rotation around the template. *EMBO J.* 11:667–672.

Trifonov, E. N., R. K.-Z. Tan, and S. C. Harvey. 1987. Static persistence length of DNA. *In* DNA Bending and Curvature. W. K. Olson, M. H. Sarma, and M. Sundaralingam, editors. Adenine Press, Albany.

Vologodskii, A. V., S. D. Levene, K. V. Klenin, M. D. Frank-Kamenetskii, and N. R. Cozzarelli. 1992. Conformational and thermodynamic properties of supercoiled DNA. *J. Mol. Biol.* 227:1224–1243.

White, J. H. 1989. An introduction to the geometry and topology of DNA structure. *In* Mathematical Methods for DNA Sequences. M. S. Waterman, editor. CRC Press, Boca Raton.

Yang, Y., T. P. Westcott, S. C. Pedersen, I. Tobias, and W. K. Olson. 1995. Effects of localized bending on DNA supercoiling. *Trends Biochem. Sci.* 20:313–319.

Zhang, P. S., I. Tobias, and W. K. Olson. 1994. Computer simulation of protein-induced structural changes in closed circular DNA. *J. Mol. Biol.* 242:271–290.(9)